CHAPTER V

INHIBITION OF COPPER CORROSION IN 1M NITRIC ACID – ELECTRO ANALYTICAL AND THEORETICAL STUDY WITH (E)-(4-(4-METHOXYBENZYLIDENEAMINO)-4H-1, 2, 4-TRIAZOLE-3, 5-DIYL) DIMETHANOL (MBATD).

5.1 REVIEW OF LITERATURE

5.2 MEDIUM

5.3 INHIBITOR MOLECULE

5.4 RESULTS AND DISCUSSION

5.5 CONCLUSIONS

5.6 REFERENCES

The work presented in this chapter is communicated Portugaliae Electrochimica Acta.PEA – M668-11(Revision submitted).

5.1 REVIEW OF LITERATURE

Copper is one of the oldest metals that have been used by man. Pure copper is soft and malleable; an exposed surface has a reddish-orange tarnish. It is used as a conductor of heat and electricity, a building material, and a constituent of various metal alloys. The low hardness of copper partly explains its high electrical and thus also high thermal conductivity. The major applications of copper are in electrical wires (60%), roofing and plumbing (20%) and industrial machinery (15%). Copper is mostly used as a metal, but when a higher hardness is required it is combined with other elements to make an alloy (5% of total use) such as brass and bronze. A small part of copper supply is used in production of compounds for nutritional supplements and fungicides in agriculture. Machining of copper is possible, although it is usually necessary to use an alloy for intricate parts to get good machinability characteristics. The electrical properties of copper are exploited in copper wires and devices such as electromagnets. Integrated circuits and printed circuit boards increasingly feature copper in place of aluminium because of its superior electrical conductivity. Heat sinks and heat exchangers use copper as a result of its superior heat dissipation capacity to aluminium. Vacuum tubes, cathode ray tubes, and the magnetrons in microwave ovens use copper, as do wave guides for microwave radiation. Copper is one of the most important constituents of carat silver and gold alloys and carat solders used in the jewelry industry, modifying the color, hardness and melting point of the resulting alloys. Copper proteins have diverse roles in biological electron transport and oxygen transportation (Haemocyanin).

L. Larabi et al. studied corrosion inhibition of copper in HCl using 2-mercapto-1- methylimidazole by dc polarization, a.c impedance and weight loss techniques. Adsorption studies obeys Langmuir adsorption isotherm. Polarization studies reveal mixed type behaviour, but the anodic effect is more pronounced. The reactivity of the compound was analyzed through Fukui indices, which are reactivity descriptors derived from density functional theory (DFT) , to explain the higher efficiency of this compound as corrosion inhibitor compared to other imidazole derivatives [1]. M Mihit et al. studied

the effect of some tetrazole compounds on corrosion inhibition of copper in HNO_3 solution at various temperatures using gravimetric and electrochemical techniques [2]. A. Fiala et al. investigated the inhibition of copper corrosion in nitric acid solution by ketene dithioacetal derivatives by weight loss, potentiodynamic polarization, scanning electron microscopy and energy dispersive X- ray fluorescence. Polarisation studies reveal that the inhibitors are cathodic in nature.SEM and energy dispersive x-ray (EDAX) examination of copper surface revealed that these compounds act by adsorption on the surface to form a protective film. The presence of the adsorbed organic compound on the electrode surface was confirmed by XRF investigation [3].

S.El Issami, L.Bazzi, M.Mihit, B.Hammouti studied triazolic compounds as corrosion inhibitor for copper in HCl at various temperatures using gravimetric, electrochemical measurements and semi-empirical molecular orbital theory [4]. Raatat M. Issa et al. conducted quantum chemical studies on the inhibition of copper surface by substituted uracils using density functional approach B3LYP/6-31G calculation. The calculated quantum chemical parameters correlated to the inhibition efficiency of the molecules. Study of adsorption of inhibitor on the metal surface shows that the adsorption through the thiocarbonyl functional group which agrees the experimental observations [5]. K Barouni et al. studied the inhibitive effect of some amino acids as corrosion inhibitors for copper in nitric acid solution using weight loss and electrochemical polarization measurements. The correlation between the quantum chemical calculations and inhibition efficiency was discussed using semi empirical methods (AMI and MNDO) [6].

S.M.Milic et al. studied some aspects of copper corrosion in presence of benzotriazole and chloride ion in a sodium tetraborate (borax) solution using polarization and adsorption studies. The compounds obey Langmuir adsorption isotherm model [7].

Yong-Ming Tang et al. reported phenyl substituted amino thiadiazole as corrosion inhibitor for copper in 0.5 M H_2SO_4 using potentiodynamic polarization and electrochemical impedance spectroscopy measurements. The

value of free energy of adsorption from Langmuir adsorption isotherm indicates the physisorption mechanism of the inhibitor. The correlation between inhibition efficiency and quantum chemical parameters has been investigated by PM3 quantum chemical calculation [8].

K.F. Khaled et al. studied some benzotriazole derivatives as corrosion inhibitors for copper in 1M HNO_3 by experimental and quantum chemical molecular dynamics approach. Quantum chemical calculations show that the benzotriazole ring and heteroatom are the active sites of the inhibitors [9]. K.F. Khaled studied corrosion control of copper in nitric acid solutions using some amino acids by weight loss, d.c polarization and a.c impedance techniques. The reactivities of the compounds were analysed through Fukui functions. Simulation techniques incorporating molecular mechanics and molecular dynamics were used to simulate the adsorption of L-methionine derivatives on copper (II) surface in nitric acid [10].

M. Mihit et al. studied the inhibition of the corrosion of copper and zinc in HNO_3 solution using (1, 2, 3, 4- tetrazoles and its derivatives) by electrochemical technique and quantum chemical calculations. The results reveal that the addition of these compounds reduces preferentially the corrosion of copper rather than that of zinc. Relationship between molecular structure and their inhibition efficiency was established by quantum chemical calculations using the density functional theory (DFT) [11].T.T Qin et al. conducted corrosion inhibition studies of copper by 2, 5-dimercapto-1,3,4-thiadiaole (DMTD) monolayer in 0.5 M HCl using cyclic voltammetry , polarization and impedance techniques. Surface observation was performed using scanning electron microscope and molecular simulation has been used to simulate adsorption model of DMTD molecule on Cu(II) surface [12].

5.2 MEDIUM

The medium for the study was prepared from reagent grade HNO_3 (E.merk) and double distilled water. All the tests were performed in aerated medium at different temperatures under normal atmospheric pressure.

5.3 INHIBITOR MOLECULE

The inhibitor, (E)-(4-(4-methoxybenzylideneamino)-4H-1, 2, 4-triazole-3, 5-diyl) dimethanol (MBATD) was prepared by condensing 4-amino-4H-1, 2, 4-triazole-3, 5-dimethanol with p-methoxy benzaldehyde. The former compound was synthesized by refluxing hydrazine hydrate and glycolic acid (E.merk) [13-15].Synthesis of the molecule is given in Scheme 5.1. The compound is soluble in 1 M HNO_3 at room temperature. The structure of the compound is given in Fig.5.1.

5.4 RESULTS AND DISCUSSION

5.4.1 Potentiodynamic Polarization Studies

The potentiodynamic polarization studies were performed by sweeping the potential between –250 mV and +250 mV at a scan rate of 1000 mV/ minutes (16mV/sec).Tafel polarization curves for copper in unstirred 1 M HNO_3 solution in the absence and presence of various concentrations of MBATD at 303, 313 and 323 K are presented in Fig.5.2(a-c). According to corrosion theories [16-17], the rightward shift of the cathodic curves reveal, that the corrosion is mainly accelerated by cathodic reactions. Being a strong oxidizing agent, HNO_3 is capable of attacking copper. The Tafel polarization curves exhibit no steep slope in the anodic range, proves that no passive film is formed on the copper surface. As a result, copper may directly dissolve in 1 M HNO_3 solution. Copper is corroded to Cu^{2+} in HNO_3 solutions, and no oxide film is formed to protect the surface from the attack of the corrosive medium. Copper dissolution is thus expected to be the dominant reaction in HNO_3 solution. The electrochemical reactions for copper in 1 M HNO_3 solution may be described as follows:

Anodic reaction

$$Cu \rightarrow Cu^{2+} + 2e^- \quad (4)$$

Cathodic reactions:

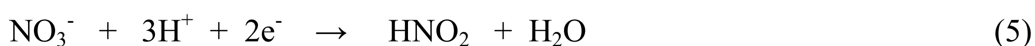

$$NO_3^- + 3H^+ + 2e^- \rightarrow HNO_2 + H_2O \quad (5)$$

$NO_3^- + 4H^+ + 3e^- \rightarrow NO + 2H_2O$ (6)

$O_2 + 4H^+ + 4e^- \rightarrow 2H_2O$ (7)

Electrochemical potentiokinetic parameters like corrosion potential (E_{corr}), cathodic and anodic Tafel slopes (β_c and β_a) and corrosion current density (i_{corr}) obtained from Tafel extrapolation of the polarization curve at 303 ,313 & 323 K were given in Table V.1. The changes in the values of the anodic and cathodic Tafel slopes (β_a & $\beta_{c)}$ suggest that MBATD act as a mixed type inhibitor. The presence of defects on the metal surface permits free access to H^+ ions and encourage the dissolution process of the metal [18-19]. The surface coverage increases with the inhibitor concentration. This film reduces the active surface area available to the corrosive medium and delays the gas evolution and copper dissolution [20].

5.4.2 Electrochemical Impedance Spectroscopy

In order to understand the adsorption and inhibition mechanism of MBATD on copper surface, electrochemical impedance spectroscopy measurements were performed to the copper/electrolyte solution interface. Electrochemical impedance spectroscopy (EIS) measurements were carried out in the frequency range 10 kHz to 0.1 Hz with amplitude of 5mV (RMS) using a.c signals at open circuit potential. The Nyquist plots and the representative Bode diagrams for the uninhibited 1 M HNO_3 and solution containing different inhibitor concentrations at various temperatures are given in Fig.5.3 (a-c) & 4(a-c).The Nyquist plots display a capacitive loop at high frequencies (may be due to charge transfer of the corrosion process) and a straight line at low frequencies (may be due to diffusion of soluble reactant or product species). It is evident from Fig.5.3(a-c) that the impedance loops measured are depressed semi-circles with their centers below the real axis. This "dispersing effect" is mainly due to the roughness and other in- homogeneities of the electrode surface [21-25]. So one constant phase element (Q) is substituted for the capacitive element in the equation to get a more accurate fit. The impedance of a constant phase element is described by the expression:

$$Z_Q = Y_0^{-1} (j\omega)^{-n}$$

where Y_0 is a proportional factor, n has the meaning of a phase shift. For n = 0, Q represents a resistance, for n = 1, a capacitance, for n = 0.5, a Warburg element and for n = -1 an inductance. According to Hsu and Mansfeld [26], the values of the double layer capacitance (C_{dl}) can be obtained from the equation:

$$C_{dl} = Yo(\omega_m^{''})^{n-1}$$

where $\omega_m^{''}$ is the frequency at which the imaginary part of the impedance has a maximum.

Charge transfer resistance (R_{ct}) and double layer capacitance (C_{dl}) were given in Table V.2. It is observed that the values of the polarization resistance increase with inhibitor concentration. The inhibition efficiencies calculated from EIS studies, show the same trend of polarization measurements. The small difference in the inhibition efficiency of these two methods may be attributed to the different surface status of the electrode in these two measurements. EIS measurements were performed at the rest potential, while in polarization measurements the electrode surface was polarized due to high over potential, non-uniform current distributions resulted from cell geometry, solution conductivity, counter and reference electrode placement etc. and will lead to the difference between the electrode area actually undergoing polarization and the total area [27].As it can be seen from Table V.2, the C_{dl} values tend to decrease with the increase of the inhibitor concentration. The decrease in the C_{dl}, which can result from a decrease in local dielectric constant and/or an increase in the thickness of the electrical double layer, suggests that MBATD molecule functions by adsorption at the metal/solution interface [28].

5.4.3 Adsorption Isotherm and Thermodynamic Parameters

From attempts to fit the θ values to different isotherms, the best-fit result obtained with the Langmuir isotherm. The plot of (C_{inh}/θ) versus C_{inh} gave a straight line at various temperatures (Fig.5.5). The values of linear regression coefficients (R^2) confirming that the adsorption of MBATD follow Langmuir

adsorption isotherm. The free energy of adsorption (ΔG^{o}_{ads}) is related to the adsorption constant (K_{ads}) with following equation [29].

$$K_{ads} = \frac{1}{55.5}\exp(\frac{-\Delta G^{o}_{ads}}{RT}) \quad (10)$$

where R is the universal gas constant, T is the thermodynamic temperature and 55.5 is the concentration of water in the solution expressed in mol^{-1}.The values of free energy of adsorption and adsorption constant are listed in TableV 3.The negative values of ΔG^{o}_{ads} and the higher values of K_{ads}($\geq 100 M^{-1}$) ensures the spontaneity of the adsorption process and are characteristics of strong interaction and stability of the adsorbed layer [30]. It is generally accepted that the values of ΔG^{o}_{ads} up to -20 kJ/mol are consistent with electrostatic interaction between the charged molecules and the charged metal (physisorption), and the value around -40 kJ/mol or higher are associated with chemisorption due to the transfer of electrons from organic molecules to the metal surface to form a coordinate type of bond [31]. The value of calculated ΔG^{o}_{ads} corresponding to MBATD is between -32 $kjmol^{-1}$ and -33 $kjmol^{-1}$.This indicates that the adsorption is not a simple physical adsorption but it may involve some other interactions also. These thermodynamic parameters are important for studying the mechanism of corrosion inhibition. The heat of adsorption (ΔH^{0}_{ads}) is calculated using the Van't Hoff equation [32]

$$\ln K_{ads} = \frac{-\Delta H^{0}_{ads}}{RT} + \text{constant} \quad (11)$$

To calculate the heat of adsorption, ln K_{ads} and 1/T was plotted and is given in Fig.5.6. From the straight line graph the slope ($-\Delta H^{0}_{ads}$/R) and intercept (ΔS^{0}_{ads}/R+ln1/55.5) values are calculated. The calculated values of heat of adsorption and entropy of adsorption are given in Table V.3. The negative sign of ΔH^{0}_{ads} indicates that the adsorption of inhibitor molecule is an exothermic process. The value of ΔS^{0}_{ads} in the presence of the inhibitor is

positive meaning that an increase in disordering takes place on going from reactants to the metal adsorbed reaction species [33].

5.4.4 Effect of Temperature and Kinetic Parameters

The effect of temperature on various corrosion parameters like E_{corr}, i_{corr} and % IE were studied in 1M HNO_3 at three different temperatures, 303 313 and 323 K in the absence and presence of different inhibitor concentrations. Variation of temperature has almost no effect on the general shape of the polarization and impedance graphs. The results were listed in Table V.1 & 2. Inspection of these tables shows that, as the temperature increases, the values of i_{corr} increases and inhibition efficiency and surface coverage decreases. This proves that the inhibition occurs through the adsorption of MBATD on copper surface. The inhibition properties of MBATD can also be explained by kinetic model. The activation parameters were calculated from Arrhenius equation and transition state equations [34-35]:

$$i_{corr} = k \exp\left(-\frac{E_a}{RT}\right) \tag{12}$$

$$i_{corr} = \frac{RT}{Nh} \exp\left(\frac{\Delta S_a^o}{R}\right) \exp\left(-\frac{\Delta H_a^o}{RT}\right) \tag{13}$$

where E_a is the activation energy, k is the Arrhenius pre-exponential factor, T is the absolute temperature, R is the gas constant, h is plank's constant, N is Avogadro's number ΔS_a^o is the entropy of activation and ΔH_a^0 is the enthalpy of activation .

A plot of ln i_{corr} versus 1/T gave a straight line as shown in Fig.5.7. The values of activation energy obtained from the slope of the lines are listed in Table V.4**.** The increase of E_a value with MBATD may be due to either physical adsorption that occurs in the first stage or due to decrease in the adsorption of the inhibitor molecule on the copper surface with increase of temperature [36-39].

To obtain the values of enthalpy and entropy of activation processes a plot of ln (i_{corr}/T) against 1/T is constructed and given in Fig.5.8. Straight lines were

obtained with a slope of (-ΔH/R) and an intercept of [ln (R/Nh) + (ΔS/R)] and the calculated values of ΔH and ΔS are given in Table V.4. The positive signs of the enthalpies (ΔH) reflect the endothermic nature of the metal dissolution process suggesting that the dissolution of copper is slow in the presence of inhibitor [40].

5.4.5 Quantum Chemical Calculations

Quantum chemical calculations are performed to understand the effect of structural parameters on the inhibition efficiency of MBATD and study its adsorption mechanism on copper surface. The optimized structure of MBATD in its ground state is given in Fig.5.9(a).

Frontier orbital theory is useful in predicting the adsorption centers of the inhibitor molecule responsible for the interaction with surface metal atoms. It is reported that excellent corrosion inhibitors are usually those organic compounds, which are not only offer electrons to unoccupied molecular orbital of the metal, but also accept free electrons from the metal. From literature it is clear that the higher the HOMO energy of the inhibitor, the greater the trend of offering electrons to the unoccupied'd 'orbital of the metal, and higher will be the corrosion inhibition efficiency. The lower the LUMO energy, the easier the acceptance of electrons by the π orbitals of MBATD from the metal. The decrease in the LUMO-HOMO energy gap increases the efficiency of the inhibitor. The pictorial representations of the HOMO and LUMO of MBATD are given in Fig.5.9(b) & 9(c). From quantum chemical parameters it is clear that MBATD has high HOMO and low LUMO with low-energy gap and thus possesses higher inhibition efficiency.

The number of electrons transferred (ΔN) was also calculated using the quantum chemical method by the following equation:

$$\Delta N = \frac{\chi_{Cu} - \chi_{inh}}{2(\eta_{Cu} - \eta_{inh})} \quad (14)$$

where χ_{Cu} and χ_{inh} denotes the absolute electro negativity of copper and the inhibitor molecule and, η_{Cu} and η_{inh} denotes the absolute hardness of copper and inhibitor molecule respectively. These are related to electron affinity (A) and ionization potential (I).

$\chi = (I+A)/2$, $\eta = (I-A)/2$. Where A and I related to E_{HOMO} and E_{LUMO}

$I = -E_{HOMO}$, $A = -E_{LUMO}$

Using a theoretical χ value of 4.48 eV/mol according to Pearson's electro negativity scale, and η value of 0 eV/mol for copper, ΔN was calculated. Values of ΔN show that inhibition effect resulted from electron donation (Table V.5). From Lukovits's study, one can derive the conclusion that if $\Delta N < 3.6$, the inhibition efficiency increases with increasing electron-donating ability at the metal surface. Here, MBATD was the donor of electrons, and the copper oxide surface was the acceptor. MBATD was bound to the copper oxide surface, and thus forming inhibitive adsorption layer against corrosion [41-46].

5.4.6 Fukui Function and Chemical Reactivity

Fukui indices are used for predicting the preferential site of electrophilic attack at MBATD. They used widely as descriptors of site selectivity for the soft-soft reactions. According to Li and Evans, the favorite reactive site is that which possess high value of Fukui indices. For nucleophilic attack the most reactive site of MBATD is the C (17) atom and for electrophilic attack the most reactive site is the N (16) atom respectively. These results are given in Table V.7.The condensed local softness indices Sk^- and Sk^+ are related to the condensed Fukui functions. The local softness follows the same trend of Fukui functions [47-49].

5.4.7 Molecular Dynamics Simulations

Molecular dynamics simulation studies were performed for understanding the nature of interaction between MBATD and copper surface. Structure of MBATD shows that the molecule is likely to adsorb on the metal surface by

sharing electron of nitrogen atom, phenyl ring and triazole structure. The periodic boundary conditions were applied to the simulation cell and the whole system was energy optimized, and the possibility of the MBATD adsorption on the copper surface was simulated as in Fig.5.10(d). The adsorption energy, the sum of the rigid adsorption energy and deformation energy for the adsorbate components have been calculated. The rigid adsorption energy reports the energy released in kcal/mol, when the unrelaxed adsorbate components adsorbed on the substrate. The deformation energy reports the energy released when the adsorbed adsorbate components are relaxed on the substrate surface. The total energy, rigid adsorption energy, deformation energy and dE_{ad}/dN_i were calculated by the Monte Carlo simulation [50-52] for the adsorption of MBATD molecule on Cu (110) plane and are presented in Table V.6. These findings also confirm the adsorption of MBATD on copper surface.

5.4.8 Scanning Electron Microscopy

SEM was employed to explore additional information on the inhibition mechanism. The SEM micrographs of copper metal before and after exposure in 1 M HNO_3 are shown in Fig 5. 10(a) & (b).These pictures clearly show that the surface was covered with high-density pits due to the exposure of copper in nitric acid. The influence of the addition of 200 ppm MBATD on copper metal in 1 M HNO_3 is shown in Fig.5.10(c).The micrograph shows no evidence of pitting. This may be due to the adsorption of inhibitor molecules around the pits formed on the specimens in the early stages of formation (initiation and propagation).

5.5 CONCLUSIONS

- The inhibitor molecule shows very high inhibitive efficiency for copper in 1M HNO_3.
- The percentage inhibition efficiency increases with increase in concentration and decreases with temperature.
- The adsorption of MBATD on copper surface follow Langmuir adsorption isotherm. The inhibitor molecules adsorb on the copper surface and

blocking the reaction sites. The surface area available for the attack decreases with increasing inhibitor concentrations.

- Polarization studies reveal that MBATD act as a mixed type inhibitor.
- The corrosion inhibition efficiency of MBATD and the values E_{HOMO}, $E_{LUMO,}$ E_{LUMO}-E_{HOMO} and ΔN of MBATD were calculated by DFT method shows the excellent inhibitive characteristics of the molecule.
- The molecular dynamics stimulation results reveal the adsorption of MBATD molecule on the copper surface.

5.9 REFERENCES

1. Larabi.L, Benali.O, Mekelleche. S.M & Harek .Y, *Appl. Surf. Sci.* 253 (2006) 1371.
2. Mihit.M, Salghi .R & El .Bazzi .S, *Pigment and Resin Technology Bradford.* 35 (2006) 151.
3. Fiala .A, Chibani .A, Darchen. A , Boulkmah. K & Djebbar, *Appl. Surf. Sci.* 253 (2007) 9347
4. El. Issami .S, Bazzi. L, Mihit .M & Hammouti .B, *Pigment & Resin Technology , Bradford.* 36 (2007) 161.
5. Raatat .M.Issa, Mohamed .K.Awad & Faten. M. Atlam, *J. Appl. Surf. Sci*. 255 (2008) 2433.
6. Barouni K , Bazzi L ,Salghi R ,Mihit M , Hammouti B ,Albourins A & Issami S.E.I, *Mat letters.* 62 (2008) 3325.
7. Milic .S.M & Antonijevic .M.M, *Corros. Sci.* 51 (2009) 28.
8. Yong-Ming Tang, *Mater. Chem. Phys*. 116 (2009) 479.
9. Khaled .K.F, Sahar. A.Fadl- Allah & Hammouti .B, *Mater ChemPhys*. 117 (2009) 148.
10. Khaled. K.F, *Corros.Sci.* 52 (2010) 3225
11. Mihit. M, Laarej .K, Abou El .Makarim, Bazzi .L, Salghi .R & Hammouti .B, *Arabian J. of Chemistry* . 3 (2010) 55.
12. Qin .T. T, Li. j , Luo .HQ, Li .M & Li .NB, *Corros Sci.* 53 (2011) 1072.
13. Adamek .M, *collect. Czech.Chem. Commu.* 25 (1960) 1694.
14. Vreugdenhil .W, Haasnoot .J.G, Reedijk .J & Spek .A.L, *Inorg Chim. Acta.* 129 (1987) 205.
15. van Koningsbruggen.P.J, van Hal J.W, de Graff R. A. G, Haasnoot J.G & Reedijk J*, J. Chem. Soc.Dalton Trans*.(1993) 2163.
16. Jones .D.A, *Principles and prevention of Corrosion, second ed., Prentice Hall, Upper Saddle River, NJ. (*1983).

17. Khaled .K.F, Sahar .A. Fadl-Allah & B.Hammouti, *Mater Chem Phys.* 117 (2009) 151.

18. Chetouani.A, Hammouti.B, Benhadda.T & Daoudi.M, *Appl. Surf. Sci.* 249 (2005) 375.

19. El Mehdi .B, Mernari.B, Traisnel.M, Bentiss.F & Lagrenee.M, *Mater Chem Phys.* 77 (2002) 489.

20. Fuchs-Godec.R, *Colloids Surf. A: Physicochem. Eng. Aspects* 280 (2006) 130.

21. Benali .O,Larabi.L & Harek.Y , *J. of Saudi chemical society.* 14 (2010) 233.

22. Da-Quan Zhang,Qi-Rui Cai,Xian-Ming He,Li-Xin Gao & Gui Soon Kim, *Mater. Chem. Phys.* 114 (2009) 614.

23. Mansfeld.F, *Corrosion.* 37 (1981) 301.

24. MacCafferty.E, *Corros. Sci* .39 (1997) 243.

25. M.S. Morad, *Corros. Sci* .42 (2000) 1313.

26. Hsu.C.H & Mansfeld.F, *Corrosion* .57 (2001) 747.

27. Kelly.R.G, Scully J.R, Shoesmith D.W & Buchheit.R.G, *Electrochemical Techniques in Corrosion Science and Engineering, Marcel Dekker, Inc., New York. (*2002) 148.

28. Lebrini.M, Lagren .M,Traisnel. M, Gengembre.L, Vezin.H & Bentiss.F, *Appl. Surf. Sci* .253 (2007) 9267.

29. Cano .E, Polo. J.L,La. Iglesia .A & Bastidas. J.M, *Adsorption.* 10 (2004) 219.

30. Lagrenee .M, Mernari .B, Bouanis, Traisnel .M & Bentiss .F,*Corros. Sci.* 44 (2002) 73.

31. Hosseini .M, Mertens .S.F.L& Arshadi .M.R, *Corros. Sci* .45 (2003) 1473.

32. Amin .M.A, Abd El Rehim S.S & Abdel-Fatah H.T.M, *Corros. Sci.*51 (2009) 882.

33. Bouklah .M, Hammouti .B, Lagrenee .M & Bentiss .F, *Corros. Sci.*48 (2006) 2831.

34. Ostovari .A, Hoseinieh S.M, Peikari .M, Shadizadeh .S.R & Hashemi .S.J, *Corros. Sci* .10 (2009) 1016.

35. del Campo .L, Perez-Saez .R.B , Gonzalez-Fernandez .L & Tello .M.J, *Corros. Sci.* 51 (2009) 707.

36. Noor.E .A & Al-Moubaraki .A.H, *Mater. Chem. Phys*.110 (2008) 145.

37. Larabi L, Harek Y, Benali O & Ghalem. S, *Prog. Org. Coat.* 54 (2005) 256.

38. Larabi L, Benali O & Harek.Y, *Mater. Lett*. 61 (2007) 3287.

39. Szauer T & Brandt A, *Electrochim. Acta*.26 (2004) 1209.

40. Guan NM, Xueming L & Fei L , *Mater Chem Phys*. 86 (2004) 59.

41. Fang .J & Li .J, *J. Mol. Struct. (THEOCHEM)* 593 (2002) 179.

42. Bereket.G, Hur .E & Ogretir .C, *J. Mol. Struct (THEOCHEM).* 79 (2002) 578.

43. Zhao .P, Liang .Q & Li .Y, *Appl. Surf. Sci.* 252 (2005) 1596.

44. Pearson .R.G, *Nati. Acad. Sci.* 83 (1986) 8440.

45. Pearson .R.G, *Inorg. Chem.*27 (1988) 734.

46. Lukovits .I, Kalman .E & Zucchi .F, *Corrosion.* 57 (2001) 3.

47. Ayers .P.W & Levy .M, *Theor chem Acta* .103 (2000) 353.

48. Geerlings .P & De Proft .F, *Int J Mol. Sci.* 3 (2002) 276.

49. Li .Y & Evans .J.N.S, *J. Am. Chem. Soc.* 117 (1995) 7756.

50. Khaled .K.F , *Appl. Sur. Sci.* 255 (2008) 1811.

51. Khaled. K.F& Amin A .Mohammed,*J Appli. Electrochem* .39 (2009).

52. Khaled .K.F, *Electrochim. Acta*. 53 (2008) 3484.

TableV.1 Electrochemical parameters for copper obtained from polarization curves in 1M HNO_3 at 303, 313 & 323K.

Temp. (K)	Conc. (ppm)	E_{corr} (mV/SCE)	L.P.R (Ωcm^2)	β_a (mV/dec)	β_c (mV/dec)	i_{corr} ($\mu A/cm^2$)	C.R (mm/yr)	I.E (%)
303	Blank	-232	23	116	176	1308	14072	---
	25	-219	29	118	170	833	10.72	37
	50	-206	37	91	163	481	5.35	63
	100	-246	39	93	154	312	4.62	76
	200	-256	47	96	159	199	3.27	85
313	Blank	-164	11	115	190	2623	39.12	---
	25	-208	17	184	188	1741	27.43	34
	50	-210	29	77	155	949	10.01	64
	100	-202	38	101	150	690	8.67	74
	200	-225	45	67	143	417	6.92	84
323	Blank	-79	10	155	109	2720	60.04	---
	25	-130	12	111	102	1841	41.12	32
	50	-187	13	78	104	1092	25.56	60
	100	-147	18	41	36	712	18.14	73
	200	-128	19	41	45	543	12.81	80

Table V.2 AC impedance data of copper with MBATD in 1M HNO_3 solutions at 303, 313& 323K.

Temp. (K)	Conc. (ppm)	R_{ct} (Ω cm^2)	C_{dl} ($\mu F/cm^2$)	i_{corr} ($\mu A/cm^2$)	C.R (mm/yr)	I.E (%)
303	Blank	45	8.08	576	13.41	---
	25	70	7.27	370	8.62	36
	50	130	4.38	201	4.64	65
	100	200	2.79	130	3.02	76
	200	311	2.66	83	1.95	86
313	Blank	14	6.35	1784	40.05	---
	25	21	5.41	1180	29.69	33
	50	37	4.47	660	11.41	62
	100	58	4.14	436	9.67	75
	200	91	1.32	269	7.50	84
323	Blank	6	5.01	3894	94.58	---
	25	9	4.74	2668	65.33	33
	50	15	3.79	1574	37.39	60
	100	23	2.52	995	25.51	74
	200	31	1.14	753	19.83	80

Table V.3 Thermodynamic parameters for the adsorption of MBATD in 1M HNO_3 on the copper in presence of 200 ppm at different temperatures.

Temperature (K)	K_{ad} (M^{-1})	ΔG^0_{ads} ($kjmol^{-1}$)	ΔH^0_{ads} ($kjmol^{-1}$)	ΔS^0_{ads} ($jmol^{-1}K^{-1}$)
303	8080	-33.7888		
313	6909	-33.4630	-16.8791	52.6717
323	5264	-33.8020		

Table V.4 Activation parameters for copper in 1 M HNO_3 in absence and presence of MBATD.

Conc. (ppm)	E_a($kjmol^{-1}$)	ΔH^0_a($kjmol^{-1}$)	ΔS^o_a($jmol^{-1}K^{-1}$)
Blank	29.3792	26.8475	-95.9569
200	40.0095	37.4812	-76.7815

Table V.5 Quantum chemical descriptors for MBATD.

Molecule	μ	I	A	- χ	η	ΔN
MBATD	8.8682	2.1056	6.7365	2.3155	4.4211	0.7685

Table V.6 Various quantum chemical parameters calculated by simulation studies.

Molecule	E_{total} (kcal/mol)	$E_{adsorption}$ (kcal/mol)	$E_{rigid\ adsorption}$ (kcal/mol)	$E_{deformatio}$ (kcal/mol)	dE_{ad}/dNi (kcal/mol)
MBATD	-121.1174	-9.6631	-9.4796	-19.1423	-9.6631

Table V.7 Fukui functions and local softness values for MBATD.

Atom	f -	f+	Sk^-	Sk^+
1C	0.0109	0.0076	0.0230	0.0160
2C	0.0169	0.0078	0.0357	0.0165
3N	0.0173	0.0045	0.0365	0.0095
4N	0.0693	0.0035	0.1463	0.0074
5N	0.0505	0.0028	0.1065	0.0059
6C	0.0004	.0015	0.0008	0.0032
7C	0.0004	0.0004	0.0008	0.0008
10H	0.0006	0.0008	0.0013	0.0017
11H	0.0004	0.0002	0.0008	0.0004
12O	0.0024	0.0001	0.0051	0.0002
13O	0.0007	0.0003	0.0015	0.0006
16 N	0.1191	0.2208	0.2513	0.4659
17C	0.1813	0.0605	0.3864	0.1277
18C	0.0136	0.1117	0.0287	0.2357
19 C	0.0401	0.1081	0.0863	0.2281
20 C	0.0943	0.0039	0.1990	0.0082
22C	0.0855	0.0079	0.1804	0.0166
24C	0.1116	0.1488	0.2324	0.3140

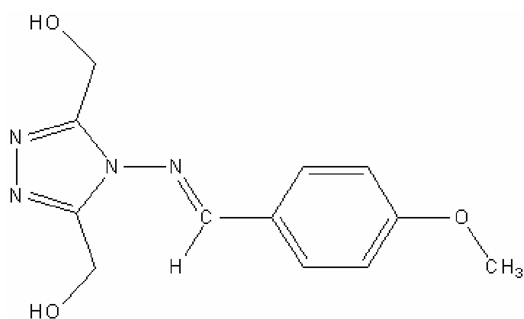

Fig.5.1 Structure of the inhibitor molecule (MBATD).

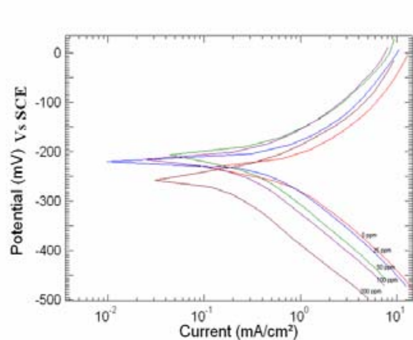

Fig.5.2a

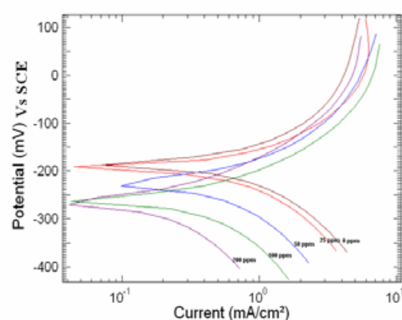

Fig.5.2b

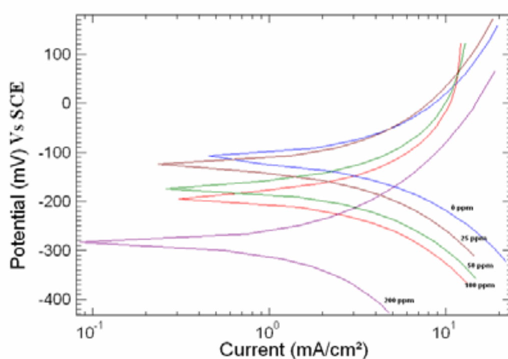

Fig.5.2c

Fig.5.2 Polarization curve of copper in 1 M HNO_3 in the absence and presence of different concentrations of MBATD at (a) 303 K (b) 313K & (c) 323K.

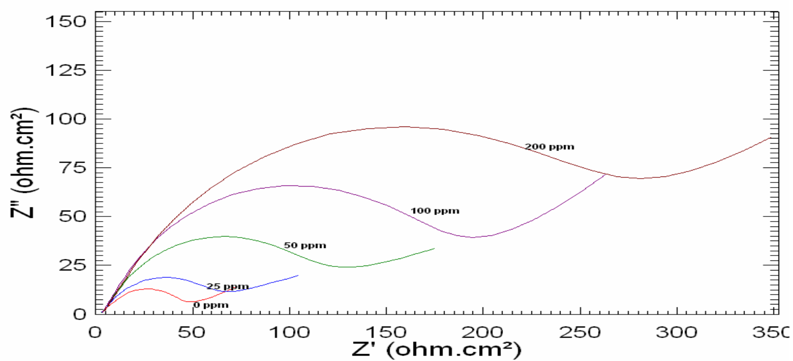

Fig.5. 3a

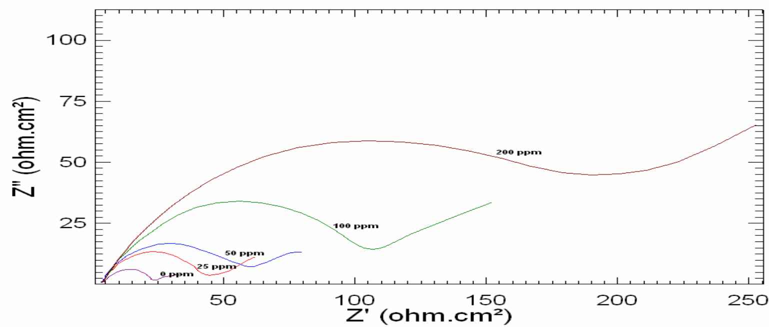

Fig.5. 3b

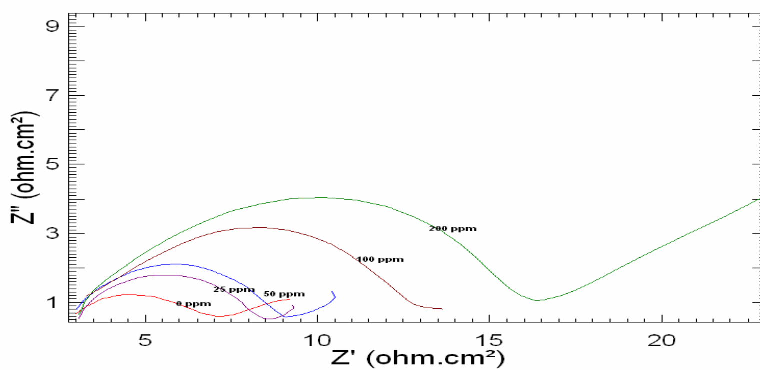

Fig.5.3c

Fig. 5.3 Nyquist plots of copper in 1 M HNO_3 in the absence and presence of different concentrations of MBATD at (a) 303 K (b) 313K & (c) 323K.

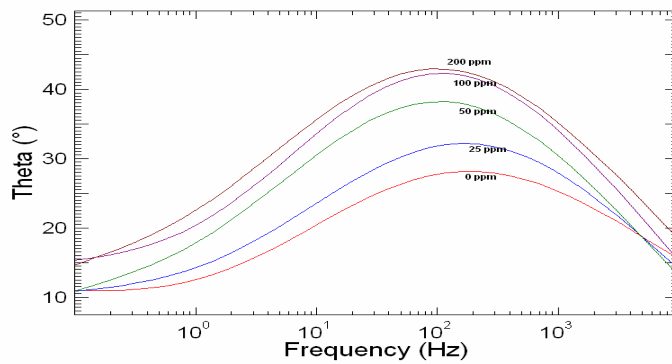

Fig .5.4a

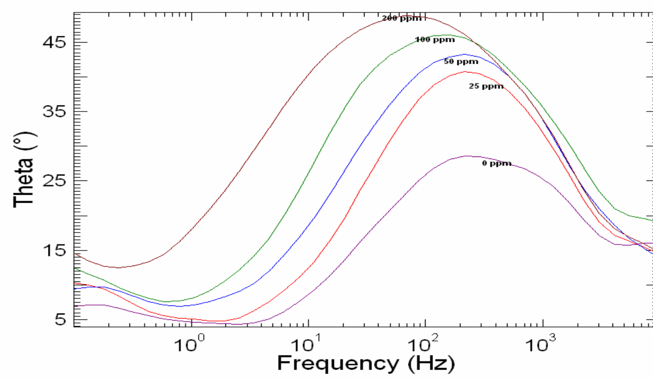

Fig .5.4b

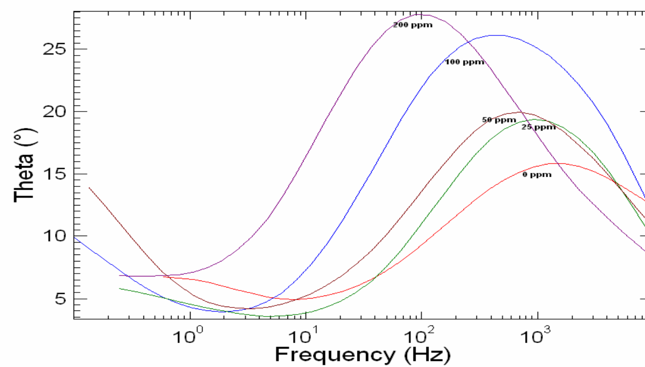

Fig .5.4c

Fig.5.4 Bode plots of copper in 1 M HNO_3 in the absence and presence of different concentrations of MBATD at (a) 303 K (b) 313K & (c) 323K.

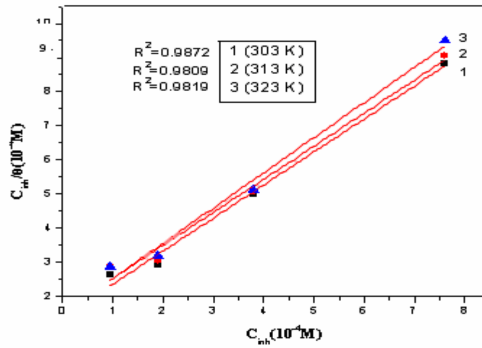

Fig.5.5 Langmuir adsorption isotherm for MBATD on copper surface in 1 M HNO_3 at 303K;(b) 313K and (c) 323K.

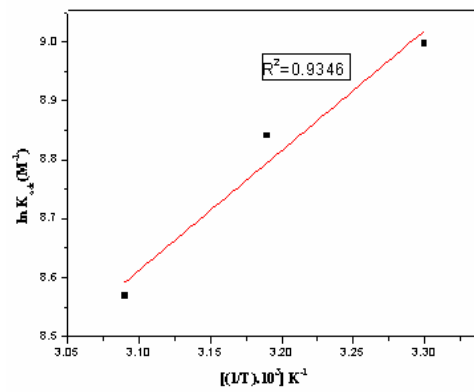

Fig.5.6 Adsorption isotherm plot for ln k_{ads} vs. 1/T of MBATD on copper in 1 M HCl.

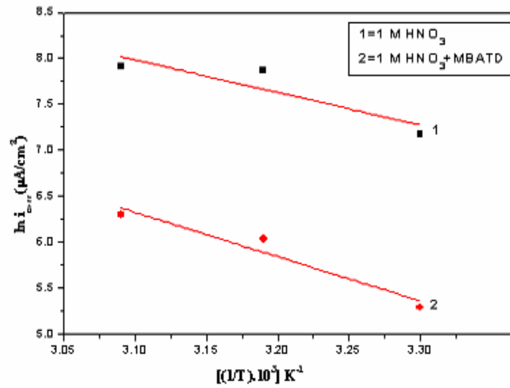

Fig.5.7 Arrhenius plots of ln(i_{corr}) versus 1/T (1) 1M HCl (2) 1M HCl+MBATD.

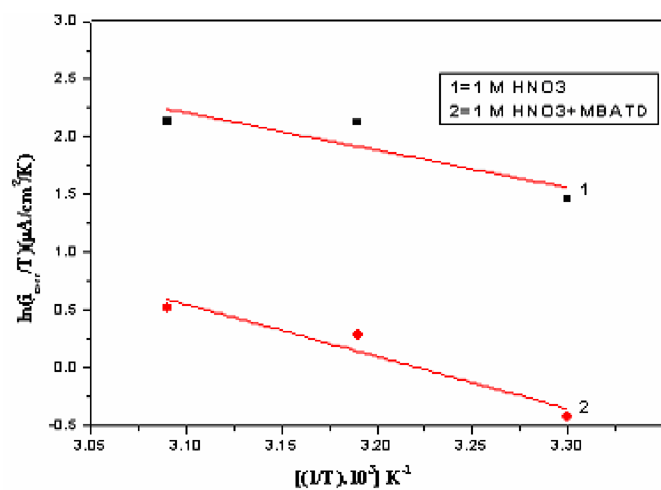

Fig.5.8 Arrhenius plots of $\ln(i_{corr}/T)$ versus 1/T. (1) 1M HCl (2) 1M HCl+MBATD.

Fig .5.9 a

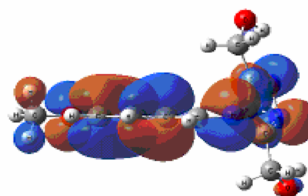

Fig.5.9 b

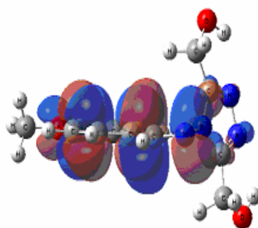

Fig.5.9c

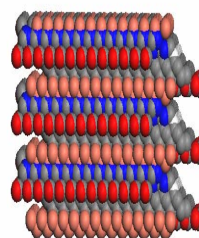

Fig.5.9d

Fig. 5.9(a) Optimized geometry of the inhibitor molecule, (b) The highest occupied molecular orbital (HOMO) of the inhibitor, (c) The lowest noccupied molecular orbital (LUMO) of the inhibitor and (d) Mode of adsorption of inhibitor molecule on copper(110) plane.

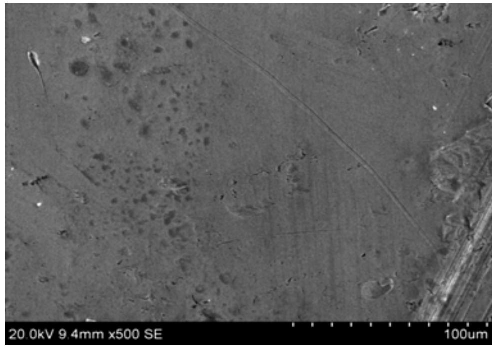

Fig.5.10a

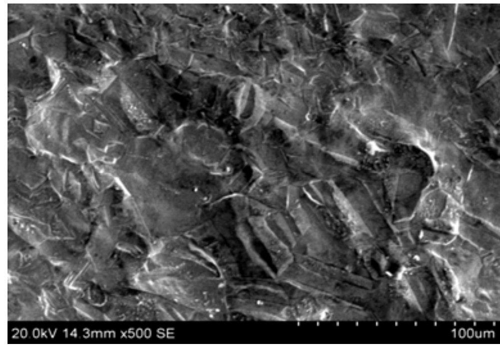

Fig.5.10b

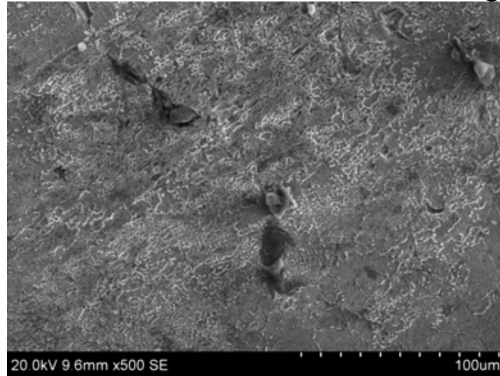

Fig.5.10c

Fig.5.10 SEM micrographs of (a) the copper metal before immersion in 1 M HNO_3; (b) after immerssion in 1 M HNO_3 and (c) after immerssion in 1 M HNO_3 containing inhibitor molecule.

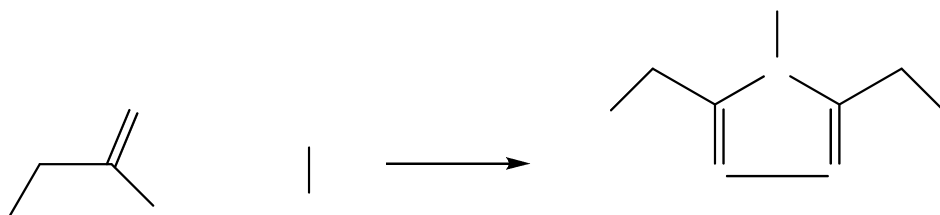

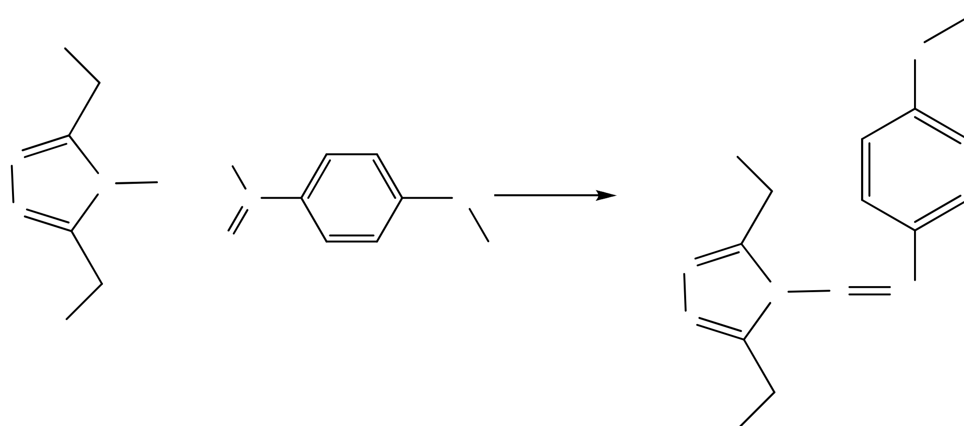

te

Scheme 5.1 Synthesis of MBATD

HO

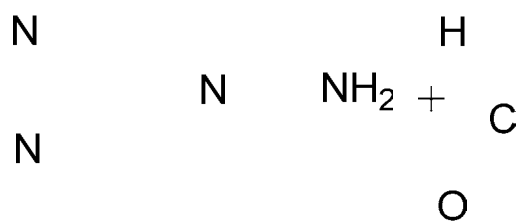

C

4-methoxybenzaldeh

HO

(4-amino-4*H*-1,2,4-triazole-
3,5-diyl)dimethanol